Hindawi
International Journal of Antennas and Propagation
Volume 2022, Article ID 2146084, 16 pages
https://doi.org/10.1155/2022/2146084

Research Article

Design and Analysis of a Dual-Band Semitransparent MIMO Antenna for Automotive Applications

Lekha Kannappan,[1] **Sandeep Kumar Palaniswamy**,[1] **Malathi Kanagasabai**,[2] **and Sachin Kumar**[1]

[1]*Department of Electronics and Communication Engineering, SRM Institute of Science and Technology, Kattankulathur, India*
[2]*Department of Electronics and Communication Engineering, College of Engineering, Guindy, Anna University, Chennai, India*

Correspondence should be addressed to Sandeep Kumar Palaniswamy; vrpchs@gmail.com

Received 13 November 2022; Revised 6 December 2022; Accepted 10 December 2022; Published 21 December 2022

Academic Editor: Trushit Upadhyaya

This paper presents the design and development of a semitransparent antenna that can be used in automotive applications to support multiple wireless services. The proposed quad-port multiple input multiple output (MIMO) antenna is comprised of four orthogonally arranged identical semitransparent antenna elements on a transparent substrate. The MIMO antenna covers the 2.4 GHz band and 3.2–15 GHz band, supporting automotive/wireless applications such as Bluetooth, Wi-Fi, intelligent transport system (ITS), advanced driver assistance systems (ADASs), vehicle to infrastructure (V2I), vehicle to vehicle (V2V), vehicle to network (V2N), and vehicle to device (V2D). The parameters such as envelope correlation coefficient (ECC), diversity gain (DG), total active reflection coefficient (TARC), and channel capacity loss (CCL) are studied to evaluate antenna diversity performance. The antenna has an ECC of less than 0.15, DG of more than 9.85 dB, TARC of less than −10 dB, and CCL of less than 0.2 bits/s/Hz. The developed antenna can be easily installed on the mirror and windshield of the vehicles. Also, the housing effect and on-vehicle performance of the antenna at various positions in a car are investigated.

1. Introduction

In modern automobiles, advanced transceiving systems are required to alert the driver about the vehicle and to ensure a safer and smoother journey. A transceiver module with an integrated antenna could be able to access multiple parameters of a vehicle, allowing for comfortable driving and passenger entertainment through infotainment services. To provide such amenities, the vehicular antenna should support multiple wireless bands such as GPS, GSM, Wi-Fi, and Bluetooth. The automotive antenna connects vehicles in order to create an intelligent transportation system (ITS), with vehicle monitoring and tracking, and a smart traffic system [1]. Customarily, each wireless service requires a dedicated antenna, which takes up a lot of chip space due to the existence of multiple radiators [2]. The installation of the antennas is also challenging due to the weight, volume, and aesthetic constraints. This problem can be solved by integrating multiple wireless services into a single antenna, eliminating the need for additional installation space.

An automotive antenna must efficiently receive signals from all directions [3]. Therefore, a multiple input multiple output (MIMO) antenna system could be useful as it can overcome the effects of multipath fading, increasing uplink and downlink data speeds without requiring additional spectrum [3]. However, in MIMO antennas, poor isolation between antenna elements increases coupling, which degrades radiation performance [4]. The coupling can be reduced by increasing the distance between the antenna elements, but this increases the size of the MIMO antenna [5]. The decoupling structures [6, 7], frequency selective surfaces/metamaterials [8, 9], defected ground plane [10, 11], and neutralization lines [12, 13] can improve isolation, but they complicate antenna design. Another method for increasing isolation is to position the antenna elements orthogonally to each other. Also, orthogonal antenna

placement achieves polarization diversity with horizontal and vertical vectors [14, 15]. The automotive antenna can be mounted on the roof using shark fin mounting [16–18], trunk, bumper, wiper, spoiler, side mirror, rear mirror, and front mirror [19]. The mounting location is determined by the type of antenna and the available space. The roof top antenna is an excellent choice for automotive applications as it can receive signals from all directions. These antennas can be designed on rigid and nontransparent substrates. In [20], a 3D antenna was designed on the FR-4 substrate for the roof top placement. In [21], an eight-port MIMO antenna was developed on the Roger substrate for the vehicle's roof. One of the challenges for automotive engineers is to deploy antenna systems without compromising the vehicle's aesthetics. This issue can be alleviated by designing antennas with transparent substrates such as soda lime glass and borosilicate glass.

This paper presents a quad-port partially transparent MIMO antenna fabricated on a soda lime glass substrate. The antenna resonates at frequencies between 2.4 GHz and 3.2–15 GHz, assisting Bluetooth, Wi-Fi, intelligent transport system (ITS), advanced driver assistance systems (ADAS), vehicle to infrastructure (V2I), vehicle to vehicle (V2V), vehicle to network (V2N), and vehicle to device (V2D). Better isolation is achieved in the proposed transparent substrate-based MIMO antenna without the use of any decoupling structures. Section 2 presents the evolution of the antenna and the surface current distributions. Section 3 discusses the radiation performance of the antenna. Section 4 investigates the antenna housing effect and directivity after installation in the vehicle.

2. Antenna Design

2.1. Unit Element. Figure 1 depicts the schematic and dimensions of the semitransparent antenna. The proposed antenna is constructed on a soda lime glass substrate of dielectric constant of 7.3 and thickness of 1.1 mm. The soda lime glass is chosen to mimic the proposed antenna with the windshield glass, maintaining the vehicle's elegance. The proposed antenna offers transparency of 33% with the soda lime glass substrate. For future consideration in achieving complete transparency, the antenna can be developed with transparent conducting oxide [22–24] as a radiator, in replacement to the copper.

Figure 2 depicts the evolution of the antenna, while Figure 3 depicts the associated S-parameters. Figure 2(a) shows a rectangular monopole antenna with a partial ground plane. The goal is to design a small antenna with multiple frequencies. The sides of the radiator and the feed line are truncated in antenna 2 and antenna 3 to improve impedance matching (see Figures 2(b) and 2(c)). The ground plane in evolution-4 is modified to achieve a wider bandwidth of 3.2–15 GHz, as shown in Figure 2(d). In the next step, a meandering slot is introduced in the radiator (see Figure 2(d)) to achieve additional 2.4 GHz (Bluetooth/Wi-Fi) resonance. The length of the slot is calculated to be $0.48\lambda_0$ (59.4 mm).

The designed antenna has a total area of 25 mm × 25 mm. The electrical characteristic of the antenna can be studied using the surface current distribution shown in Figure 4. For 2.4 GHz, the current density is given in the Figure 5. For 4 GHz, the current density is found to be high around the feed line (Figure 4(a)). The radiation intensity is found to be higher around the feed line and the truncated edges of the radiator between 6 GHz and 9 GHz (Figures 4(b) and 4(c)). The surface current distribution of the proposed prototype with and without slot is shown in Figure 5 for the frequency of 2.4 GHz. The result shows that the slot is highly responsible for the resonance of 2.4 GHz.

2.2. Parametric Analysis. The parametric analysis of the radiator for resonance of UWB and the slot for the operation of 2.4 GHz is performed. Figure 6 shows the parametric dimensional change (PDC) and its corresponding results with respect to UWB resonance. Table 1 shows the change in values of the parameter for UWB. The reflection coefficient characteristics with respect to the UWB (Figure 6(e)) shows that the variation in the parameter "G" and "W" provides better impedance matching and covers lower frequency.

Figure 7 shows the parametric analysis of the stub for the resonance of 2.4 GHz. As the length of the stub (H) increases, the resonance shifts towards the lower frequency. Table 2 shows the change in parameters for the 2.4 GHz.

2.3. MIMO/Diversity Antenna. Figures 8(a) and 8(b) depict the schematic of the proposed quad-port semitransparent MIMO antenna. The antenna is fabricated on the soda lime glass substrate, shown in Figure 8(c). The antenna elements are orthogonally placed to improve isolation and achieve polarization diversity. In automotive antennas, MIMO/diversity is important for receiving signals from all directions. The size of the MIMO antenna is $0.448\lambda_0 \times 0.448\lambda_0$.

The antenna is measured using the Anritsu MS 2037C vector network analyzer (VNA), as shown in Figure 8(d). The MIMO antenna has a −10 dB impedance bandwidth of 3.1–15 GHz and an additional resonance at 2.4 GHz (see Figure 9(a)). A better isolation can be achieved by incorporating decoupling structures into the antenna, increasing the space between the antenna elements, and orienting the antenna orthogonally. The proposed semitransparent MIMO antenna achieves isolation of greater than 15 dB over the frequency range of 2.4–15 GHz, with a minimum spacing of $0.0192\lambda_0$. In the proposed design, no decoupling structures [25–27] are used to increase isolation, and only the orthogonal orientation of the element helps in increasing interelement isolation.

Figure 10 shows the connected ground structure [28] and its corresponding reflection coefficient characteristics are shown in Figure 11. The results show that the antenna performance is not affected due to the addition of connected ground plane structure. The grounds are connected to each other with a stub of width 0.25 mm.

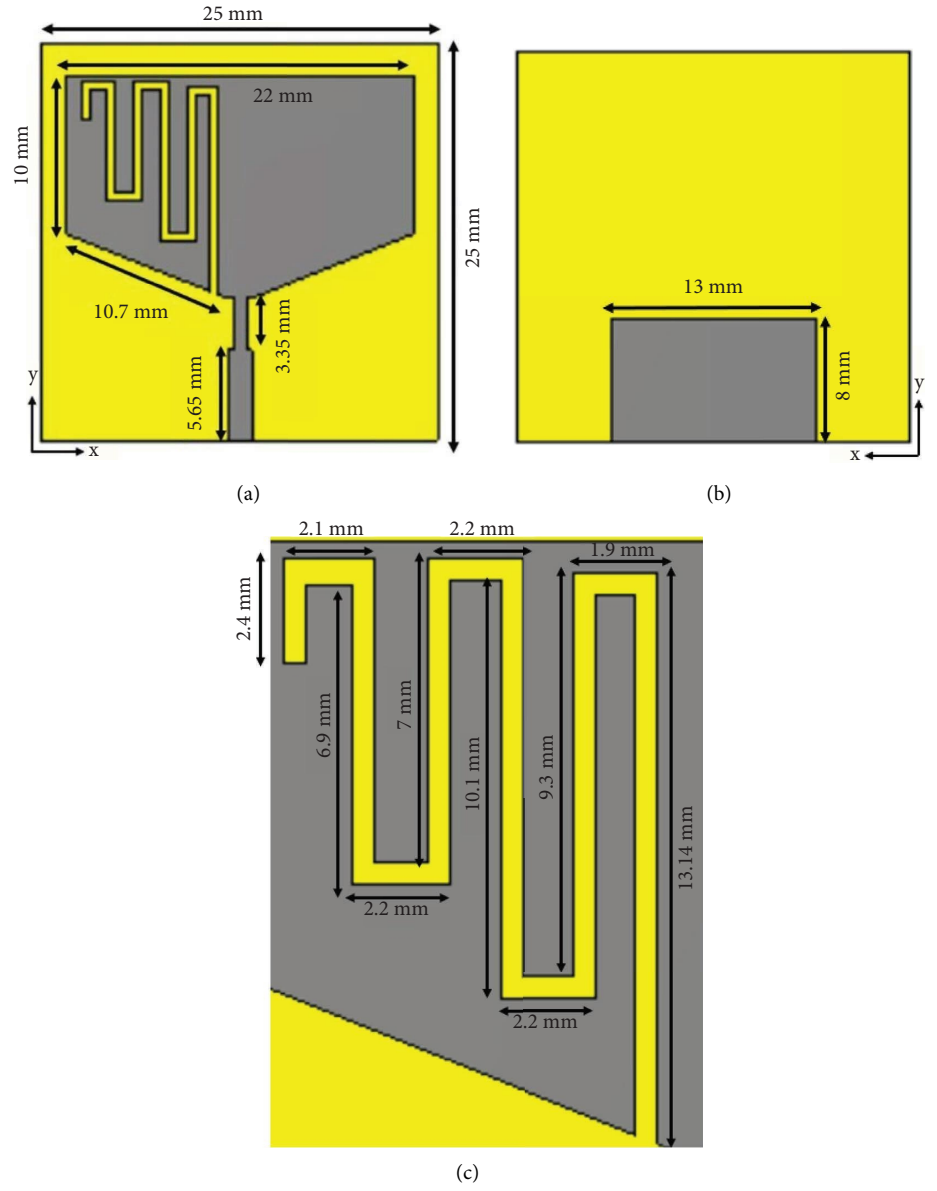

Figure 1: Schematic of the semitransparent antenna. (a) Front side. (b) Back side. (c) Dimension of the slot for 2.4 GHz.

2.4. Diversity Characteristics. Multiple antennas are required in the vehicular environment to receive signals from all directions. The parameters such as envelope correlation coefficient (ECC), diversity gain (DG), total active reflection coefficient (TARC), and channel capacity loss (CCL) are studied to evaluate the diversity functioning of the antenna [29]. ECC denotes how an antenna element in a system is independent of other antennas. The ECC is calculated using the following equation, and the practical limit of ECC is less than 0.5.

$$\mathrm{ECC} = \frac{\left|\iint\left[\overrightarrow{F_1}(\theta,\varphi).\overrightarrow{F_2}(\theta,\varphi)\right]\mathrm{d}\Omega\right|^2}{\iint\left|\overrightarrow{F_1}(\theta,\varphi)\right|^2\mathrm{d}\Omega\iint\left|\overrightarrow{F_2}(\theta,\varphi)\right|^2\mathrm{d}\Omega}, \quad (1)$$

where F_1 and F_2 are the radiated fields.

The term DG refers to an improvement in the signal-to-interference ratio without sacrificing quality, and it is also related to ECC.

$$\mathrm{DG} = 10 \times \sqrt{1 - \mathrm{ECC}^2}. \quad (2)$$

The CCL gives transmission rate and signal reliability information. It is calculated using the following equation:

$$\mathrm{CCL} = -\log_2 |\psi|^R, \quad (3)$$

where correlation matrix is given as $|\psi|^R = \begin{vmatrix} \rho_{11} & \rho_{12} \\ \rho_{21} & \rho_{22} \end{vmatrix}$.

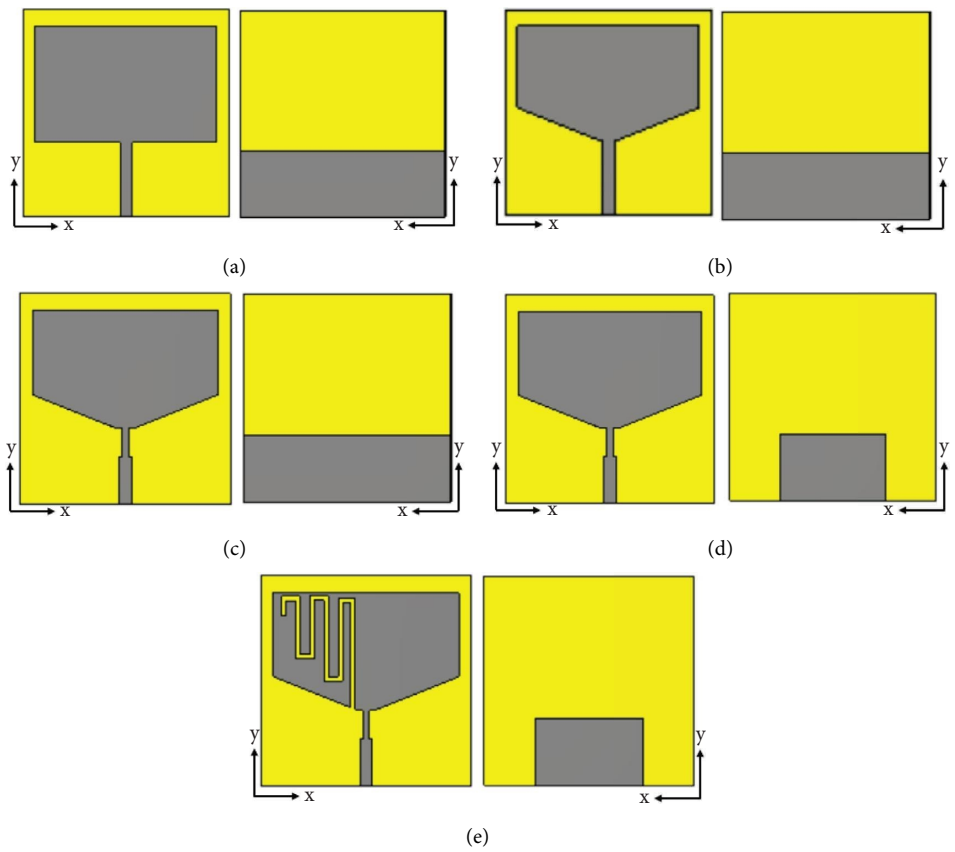

Figure 2: Design phases of the proposed antenna. (a) Antenna 1. (b) Antenna 2. (c) Antenna 3. (d) Antenna 4. (e) Antenna 5.

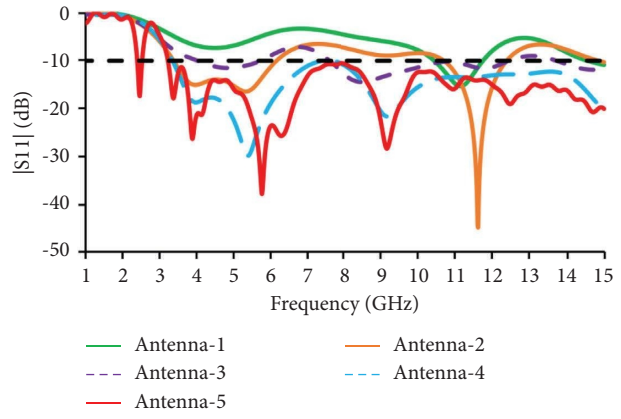

Figure 3: Reflection coefficients of the design steps.

$$\begin{aligned}\rho_{11} &= \left(1 - |S_{11}|^2 - |S_{12}|^2\right),\\ \rho_{12} &= -\left(S_{11} * S_{12} + S_{21} * S_{22}\right),\\ \rho_{21} &= -\left(S_{22} * S_{21} + S_{12} * S_{21}\right),\\ \rho_{22} &= \left(1 - |S_{22}|^2 - |S_{21}|^2\right).\end{aligned} \tag{4}$$

TARC (Γ_a^t) is the ratio of the total reflected power b_i divided by the total incident power a_i in an N-port system, where i varies from port-1 to port-4. The ECC, DG, CCL, and TARC curves are plotted in Figure 12.

$$\Gamma_a^t = \frac{\sqrt{\sum_{i=1}^{N} |b_i|^2}}{\sqrt{\sum_{i=1}^{N} |a_i|^2}}. \tag{5}$$

Table 3 shows the mean effective gain (MEG) of the semitransparent MIMO antenna. The MEG ratios of antenna 1 and antenna 2 are found to be close to unity for the desired frequencies.

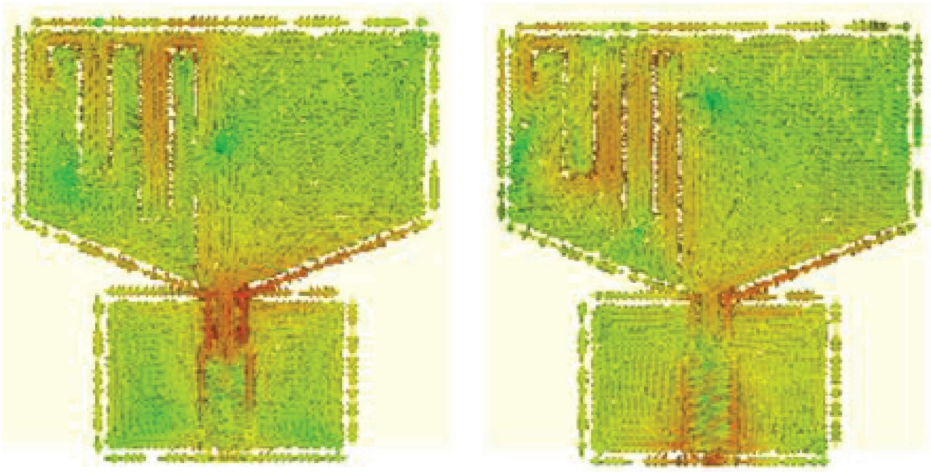

(a) (b)

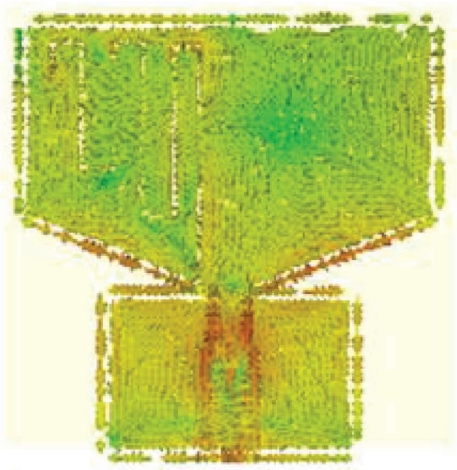

(c)

Figure 4: Distribution of the surface current at (a) 4 GHz; (b) 6 GHz; (c) 9 GHz.

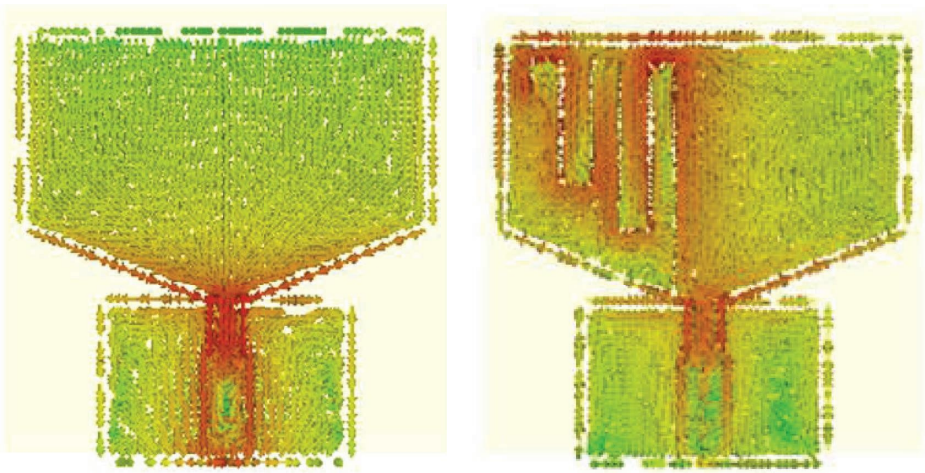

(a) (b)

Figure 5: Surface current distribution for the frequency of 2.4 GHz (a) without slot and (b) with slot.

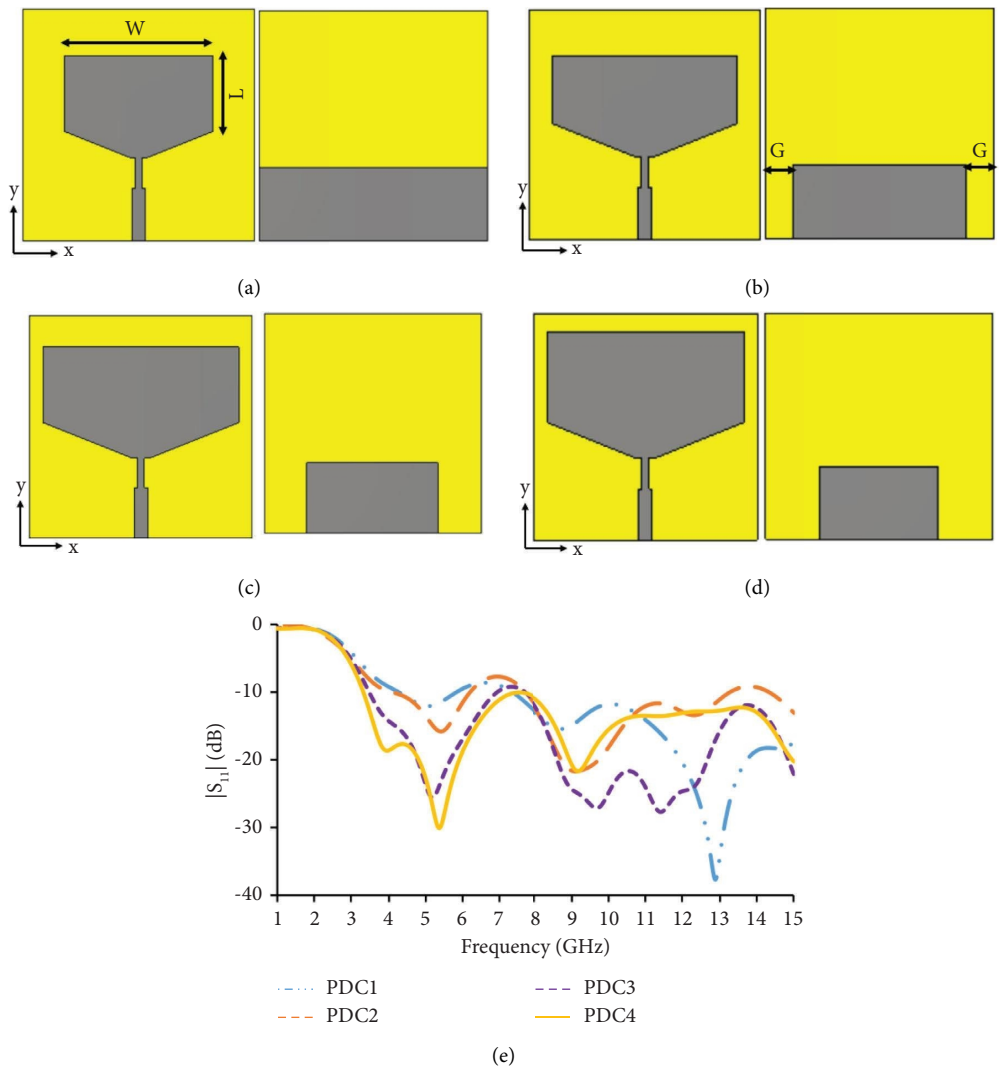

Figure 6: Parametric analysis. (a) PDC1. (b) PDC2. (c) PDC3. (d) PDC4. (e) Reflection coefficient characteristics.

Table 1: Parametric dimensional changes for UWB.

Parameters (mm)	PDC1	PDC2	PDC3	PDC4
L	7.4	7.4	8.5	10
W	16	20	20	25
G	0	3	5	6

2.5. Radiation Characteristics. Figure 13 depicts the radiation plots of the semitransparent antenna at 2.4 GHz, 4 GHz, 6 GHz, and 9 GHz frequencies. In copolarization, the transmitter and receiver have the same polarization, whereas in cross-polarization, the transmitter and receiver have different polarizations. The radiation patterns in the elevation plane (E-plane, $\varphi = 90^{\circ}$) are bidirectional, whereas the radiation patterns in the azimuth plane (H-plane, $\varphi = 0^{\circ}$) are omnidirectional.

The gain and efficiency plots of the proposed semitransparent antenna are shown in Figure 14. The maximum values of the simulated and measured gain are 2.24 dBi and 2.14 dBi, respectively. The efficiency obtained is greater than 75%.

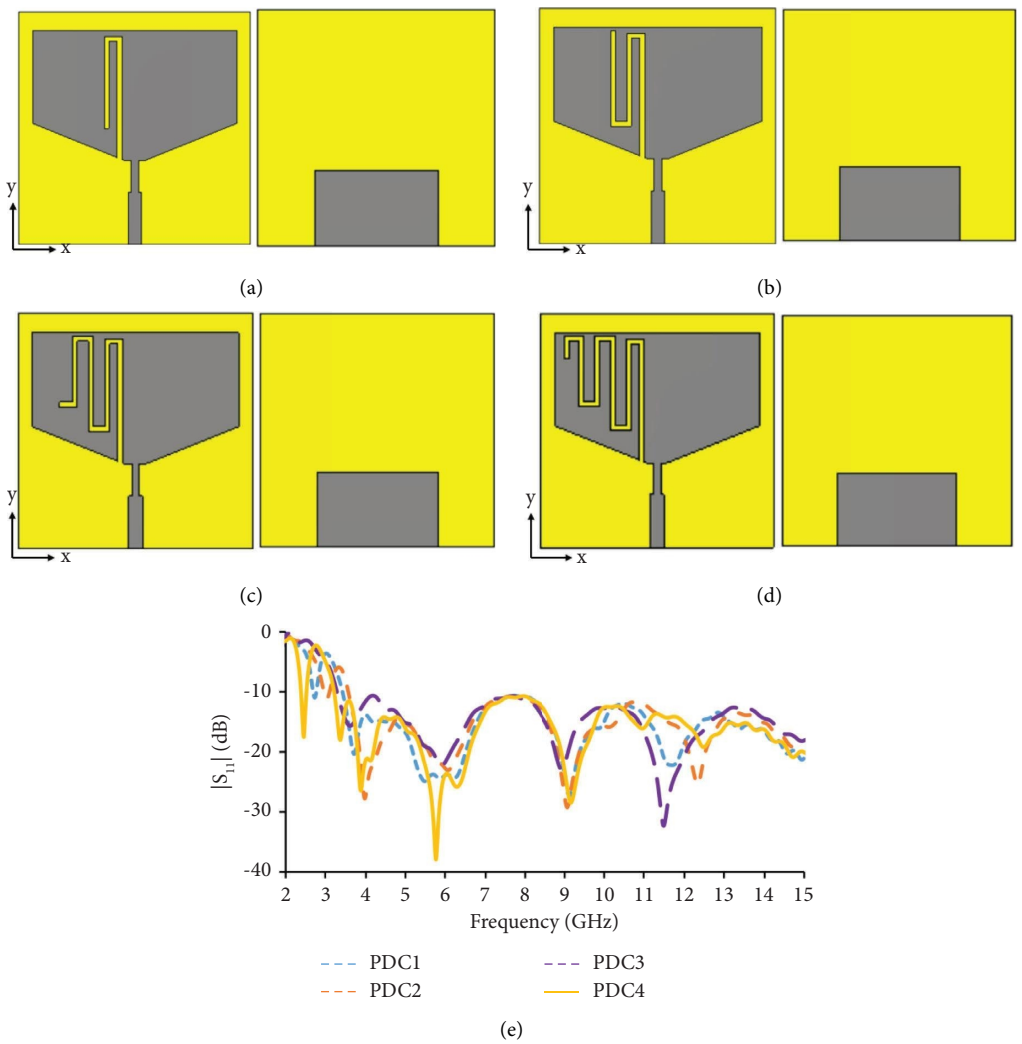

Figure 7: Parametric analysis. (a) PDC1. (b) PDC2. (c) PDC3. (d) PDC4. (e) Reflection coefficient characteristics.

Table 2: Parametric dimensional changes for 2.4 GHz.

Parameter	PDC1	PDC2	PDC3	PDC4
H (mm)	24.34	36.64	48.04	59.44

2.6. Antenna Housing Effects

2.6.1. S-Parameter and Far-Field Characteristics. The proposed semitransparent antenna is installed in the windshield of the car (Figure 15(a)), and the reflection coefficient characteristics are studied. The plot in Figure 15(b) suggests that the antenna's performance is unaffected even after installation in the windshield.

The far-field characteristics of the transparent substrate-based antenna imported into the car model are depicted in Figure 16. A Volkswagen Touareg open-source car model is used for the far-field study. The semitransparent antenna has near omnidirectional characteristics and improved directivity, as illustrated in Figures 16(a)–16(c).

2.7. Effects of Surrounding Conductors. A metal plate that acts as a large ground plane is used to study the effect of other conductors near the semitransparent MIMO antenna. The metal plate imitates the roof of the vehicle. The proposed semitransparent MIMO antenna is positioned vertically (case-1) and horizontally above metal (case-2) (see Figures 17(a) and 17(b)). The metal plate measures 40 cm × 40 cm × 5 cm. The gap between the metal plate and the semitransparent antenna element is 10 mm. Figures 17(c) and 17(d) depict the corresponding reflection coefficient characteristics.

Table 4 compares the proposed work to the previous literature. The salient features of the transparent substrate-based antenna are as follows:

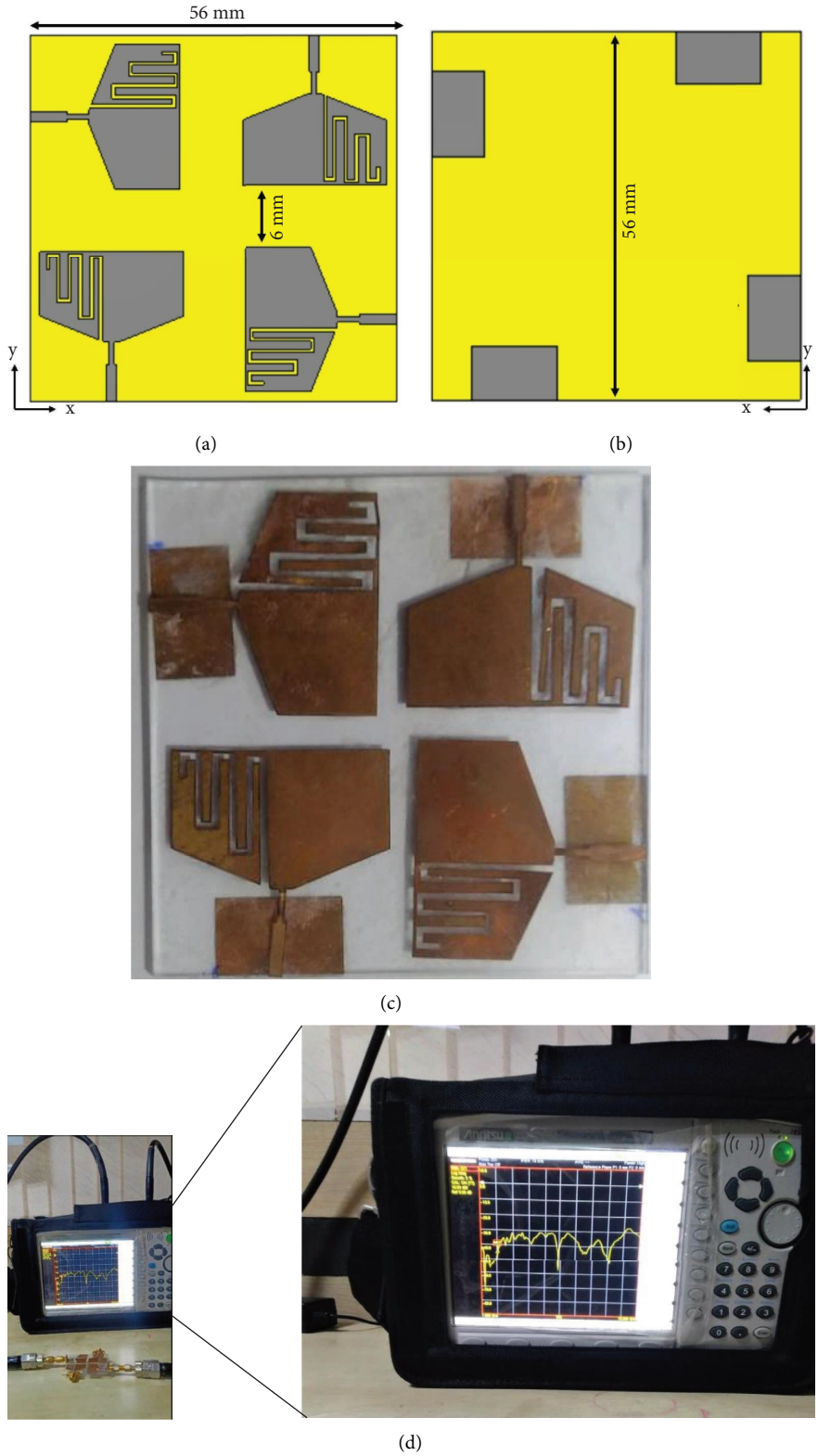

Figure 8: Proposed quad-port semitransparent MIMO antenna. (a) Front side. (b) Back side. (c) Fabricated prototype on the soda lime glass substrate. (d) Measurement (S21) using the VNA.

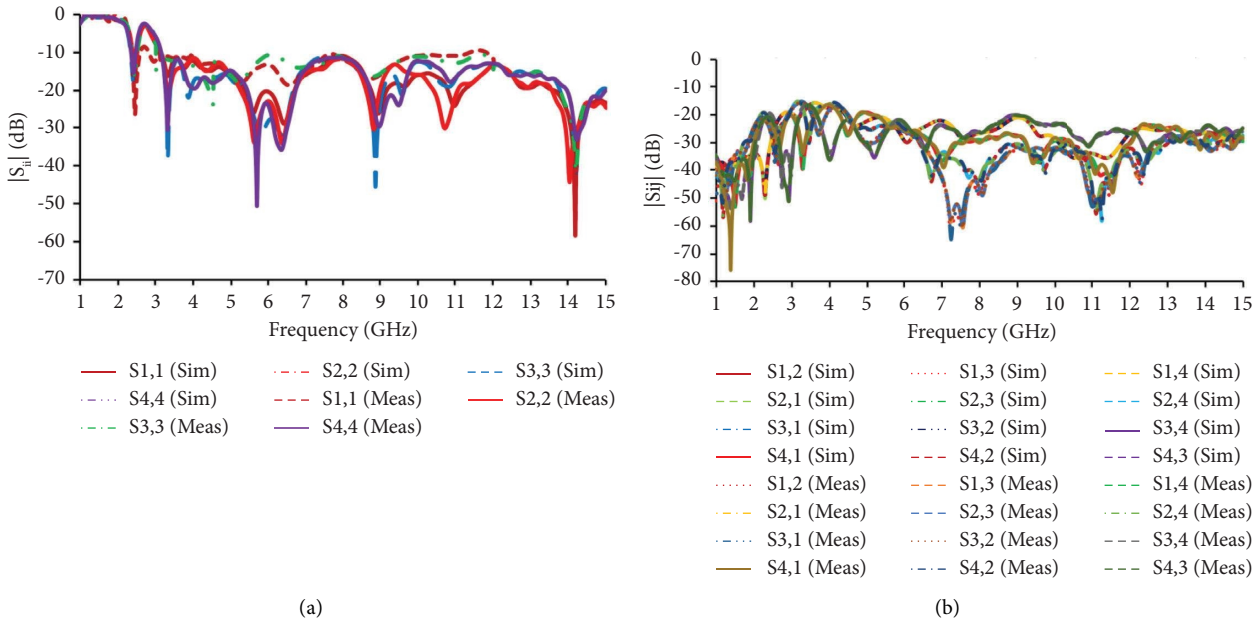

Figure 9: *S*-parameters of the semitransparent MIMO antenna. (a) Simulated (sim) and measured (meas) reflection coefficients. (b) Simulated (sim) and measured (meas) mutual couplings.

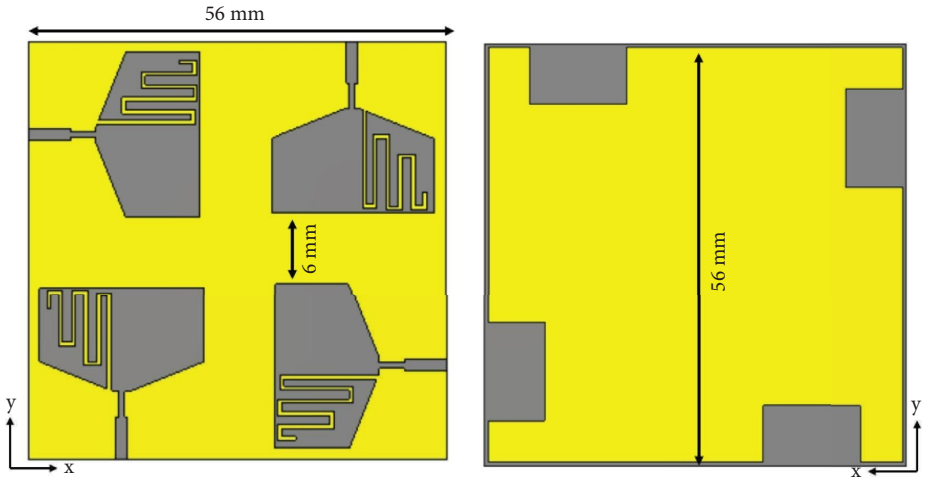

Figure 10: Connected ground MIMO structure.

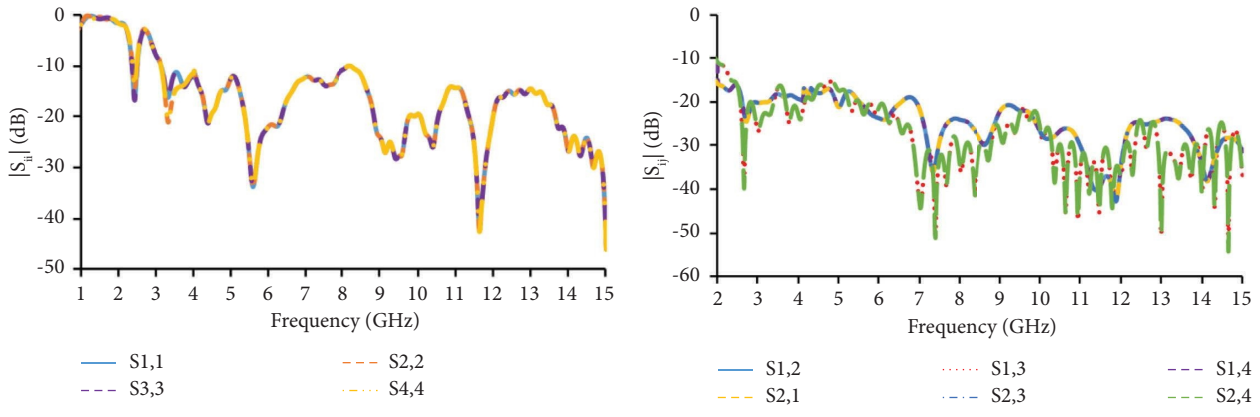

Figure 11: Continued.

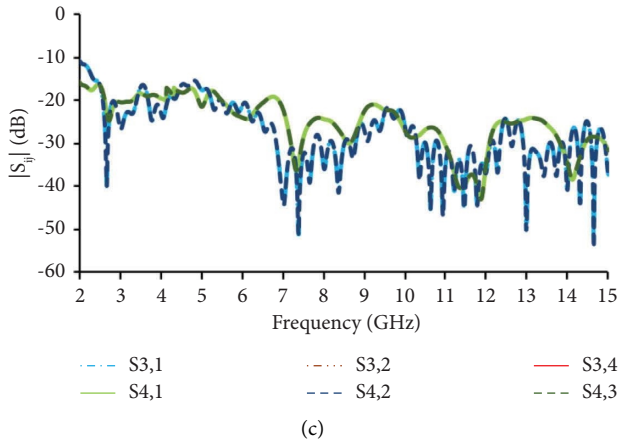

Figure 11: *S*-parameter characteristics with respect to connected ground structures. (a) Reflection coefficient characteristics. (b) Mutual coupling w.r.t antenna 1 and 2. (c) Mutual coupling w.r.t antenna 3 and 4.

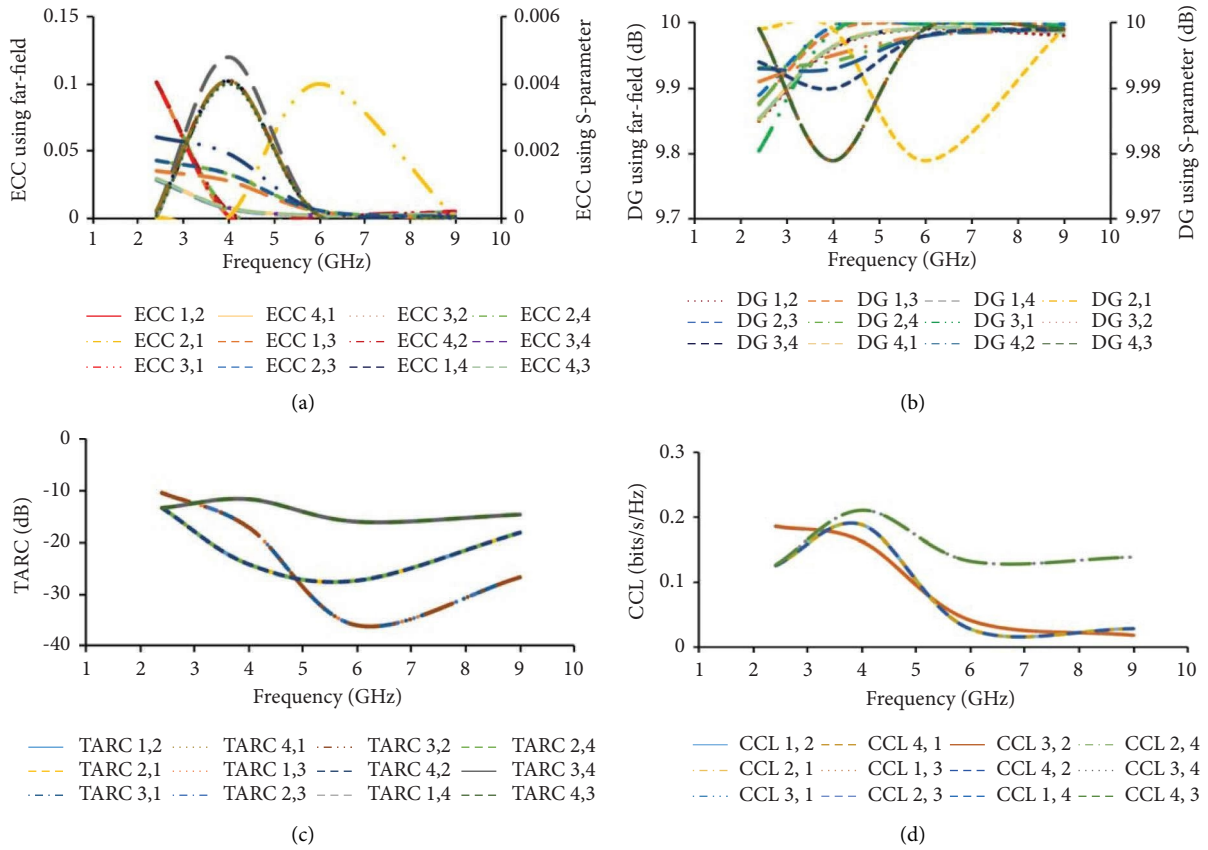

Figure 12: Diversity parameters of the semitransparent MIMO antenna. (a) ECC. (b) DG. (c) TARC. (d) CCL.

Table 3: MEG of the semitransparent MIMO antenna.

Frequency (GHz)	Isotropic XPR = 0 dB MEG_1/MEG_2	Outdoor XPR = 1 dB MEG_1/MEG_2	Indoor XPR = 5 dB MEG_1/MEG_2
2.4	1	0.978	1
4	1	0.959	1
6	1	0.9911	1
9	1	1	1

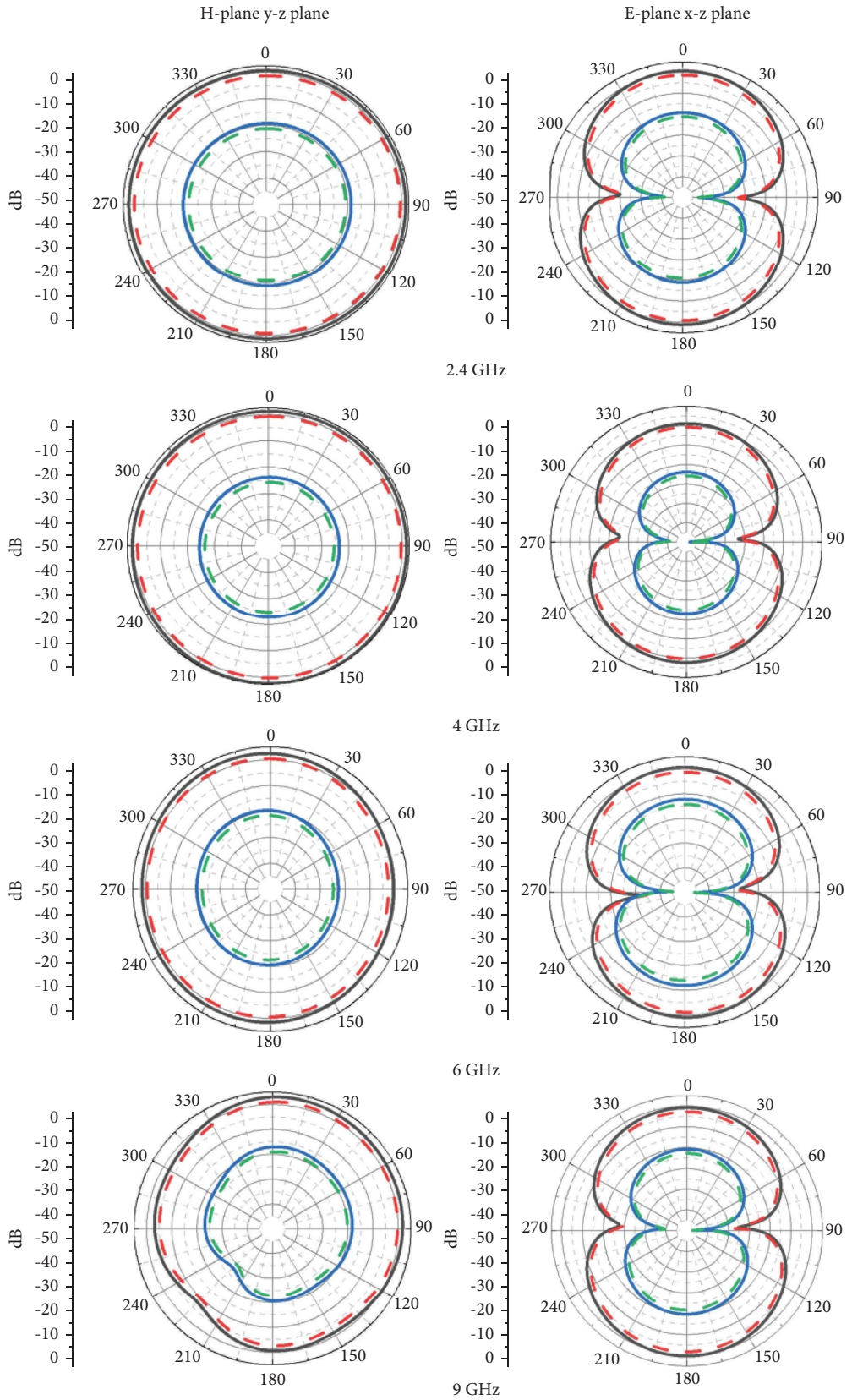

(a)

Figure 13: Continued.

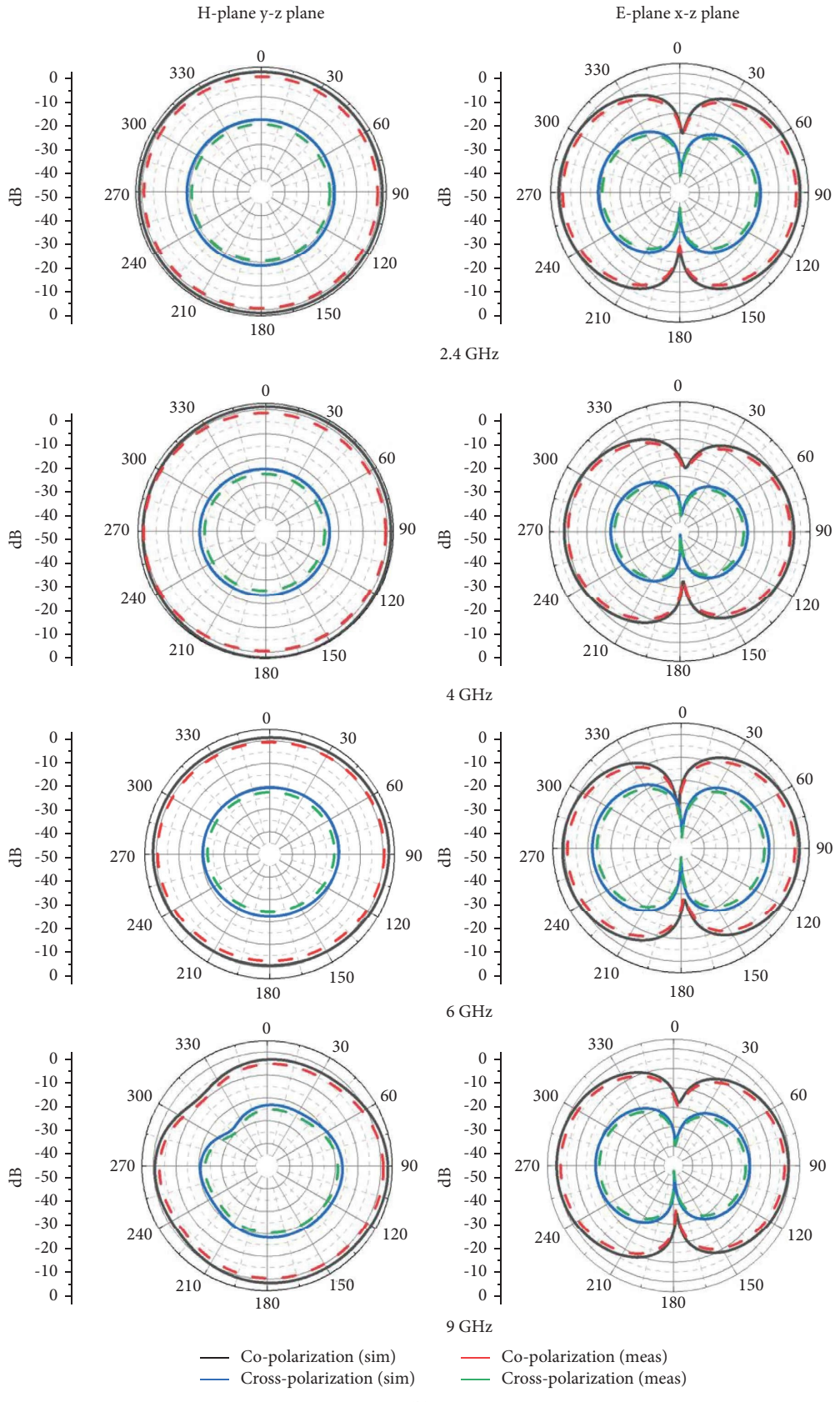

(b)

Figure 13: Radiation patterns of semitransparent antenna. (a) Antenna 1. (b) Antenna 2.

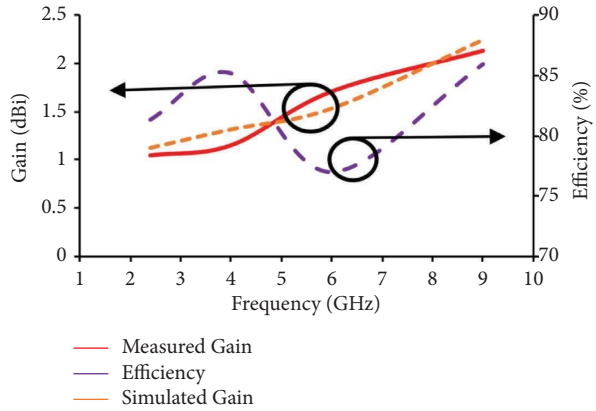

Figure 14: Gain and efficiency of the proposed antenna.

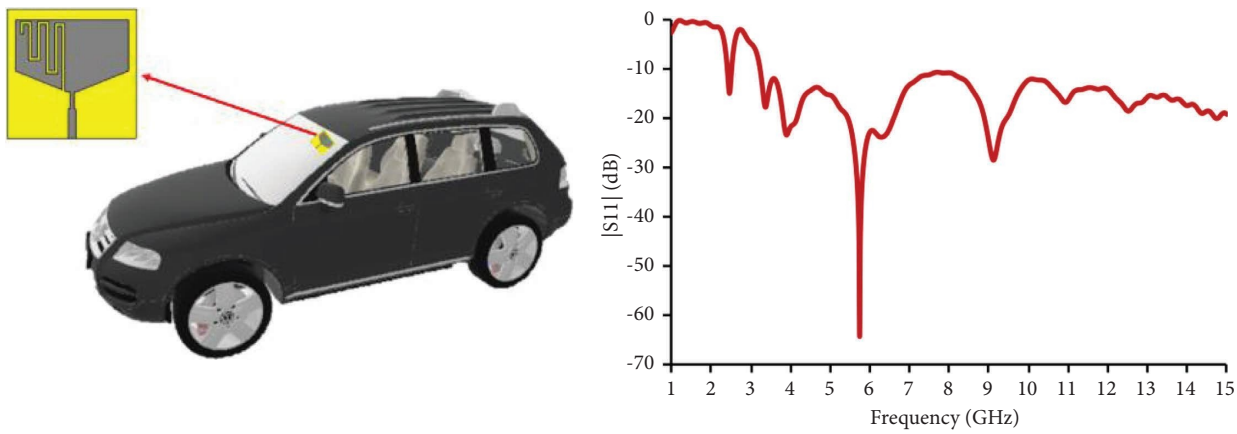

Figure 15: On-car performance of the proposed semitransparent antenna. (a) Vehicle placement. (b) Reflection coefficients related to antenna placement in a vehicle.

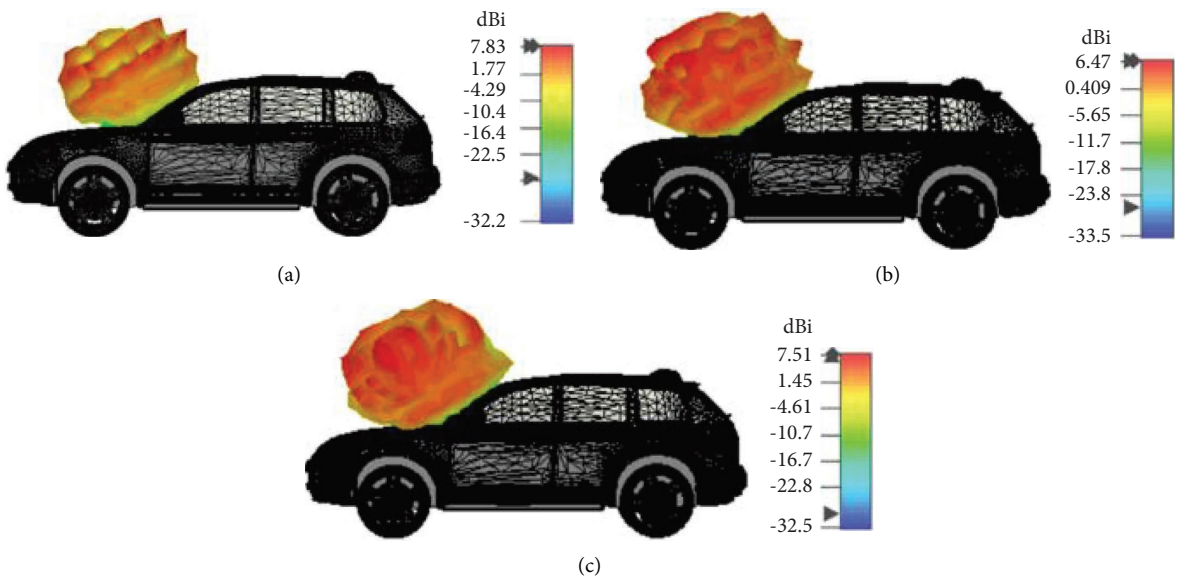

Figure 16: Directivity of the semitransparent antenna in a vehicle. (a) 2.4 GHz. (b) 4 GHz. (c) 6 GHz.

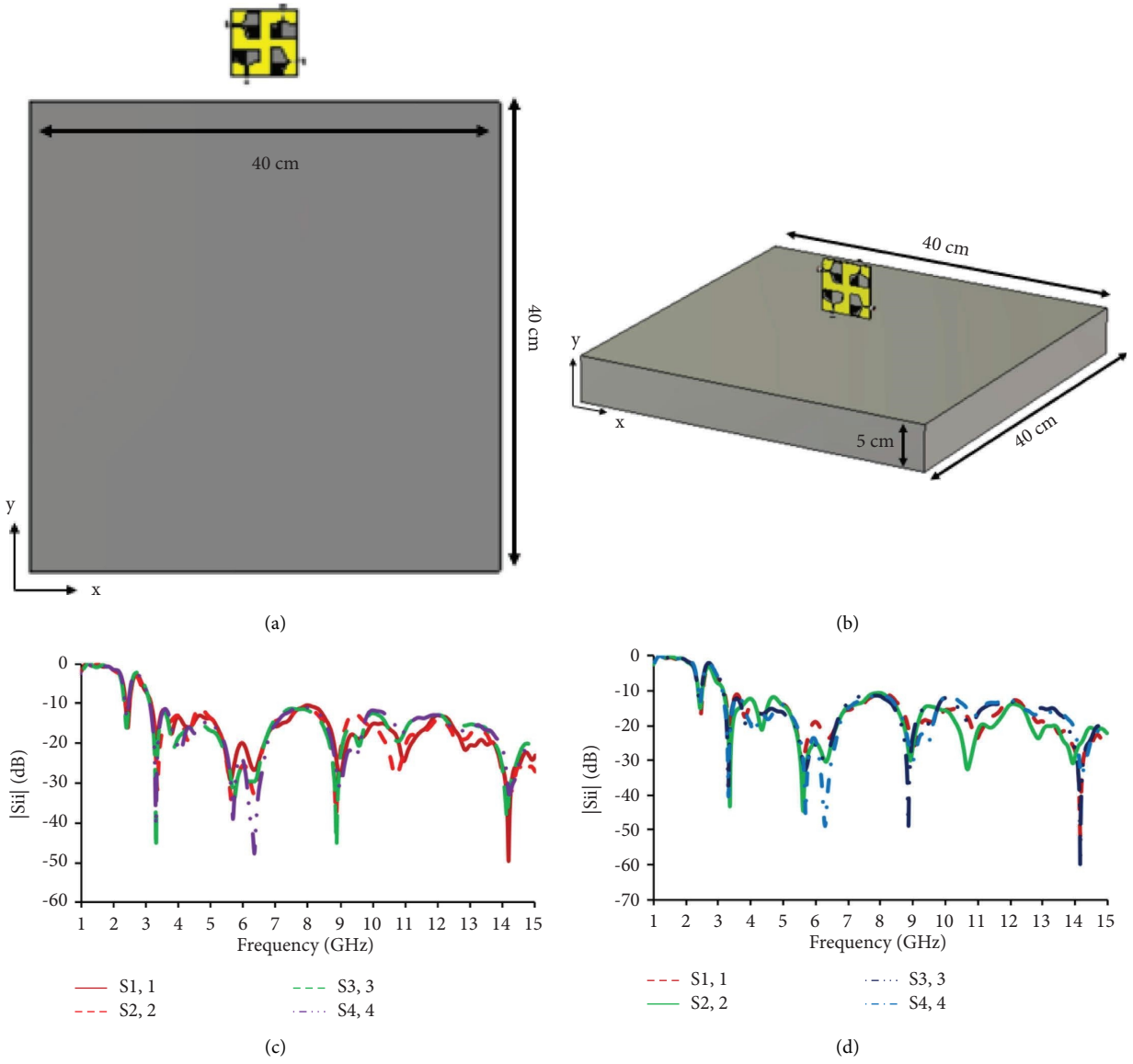

Figure 17: Effect of the metal plate on semitransparent antenna. (a) Case 1. (b) Case 2. (c) Refection coefficients of case 1. (d) Reflection coefficients of case 2.

Table 4: Comparison of the proposed semitransparent antenna over previous literature.

Ref	Dimension ($\lambda_0 \times \lambda_0$)	Substrate	Operating frequency (GHz)	ECC	DG (dB)	CCL (bits/s/Hz)	Polarization
[30]	1.01×0.677	FR-4	5.08–7.02, 2.4	—	—	—	—
[31]	0.396×0.396	FR-4	3.72–3.82, 4.65–4.76, 6.16–6.46	<0.1	>9.7	<0.8	Vertical
[32]	0.36×0.51	FR-4	2.18–2.24, 2.38–2.46, 2.65–2.70, 3.10–3.32, 3.38–3.46	0.005	>9.9	<0.35	Vertical
[33]	0.55×0.55	FR-4	2.73–10.68	—	—	—	Dual

Table 4: Continued.

Ref	Dimension ($\lambda_0 \times \lambda_0$)	Substrate	Operating frequency (GHz)	ECC	DG (dB)	CCL (bits/s/Hz)	Polarization
[34]	0.2×0.2	FR-4	1.41–1.62, 2.4–2.462, 3.1–12.8	<0.4	>9	<0.4	Dual
[35]	0.733×0.733	FR-4	5.5–9.2, 13.2–17.9, 11.5–14.6	<0.05	>9.9	—	Dual
[36]	0.93×0.93	FR-4	3.1–10.6, 3–4.5, 4.4–6	<0.15	—	—	Dual
This work	0.44×0.44	Soda lime glass	2.37–2.51, 3.2–15	<0.15	>9.85	<0.2	Dual

(i) The proposed semitransparent antenna is developed on the soda lime glass substrate with a thickness of 1.1 mm and can be installed in the mirror and windshield of the vehicle.

(ii) The proposed MIMO antenna has a dimension of $0.44\lambda_0 \times 0.44\lambda_0$, which occupies less space than other works reported in the literature [30, 32, 33, 35, 36].

(iii) Unlike [33–36], the proposed semitransparent antenna provides dual-band without any reconfigurability techniques.

(iv) Unlike previous work [30, 33], the designed semitransparent antenna operates at integrated frequencies between 2.4 GHz and 3.2–15 GHz.

(v) The vehicular environment necessitates the use of multiple antennas to receive signals from all directions. Therefore, by arranging the semitransparent antenna elements orthogonally, the antenna provides better isolation without any decoupling structures and also has two polarization vectors (horizontal and vertical).

(vi) The CCL is found to be less than 0.2 bits/s/Hz unlike [31, 32, 34].

3. Conclusion

A quad-port semitransparent MIMO/diversity antenna is presented for automobile applications. The transparent substrate does not affect the aesthetic appearance of the vehicle. The antenna supports the 2.4 GHz band and UWB. The proposed transparent substrate-based antenna is mounted in the car model and its reflection coefficient characteristics and diversity parameters are investigated. The results indicate that the diversity parameters are within the practical range. The semitransparent antenna is also tested for housing effects and on-vehicle performance. The proposed antenna can be integrated into a vehicle for automotive applications such as ITS, ADAS, traffic management, and vehicular communications.

Data Availability

The data used to support the findings of this study are available from the corresponding author upon request.

Conflicts of Interest

The authors declare that they have no conflicts of interest.

References

[1] J. Feng, G. Jiang, Y. Ding, X. Zhang, H. Liu, and Y. Fan, "Antenna performance test method and result analysis for V2X communication of connected vehicle," *Journal of Physics: Conference Series*, vol. 1607, no. 1, Article ID 012082, 2020.

[2] R. Azaro, F. De Natale, A. Massa, S. Piffer, and E. Zeni, "Design of an integrated antenna for automotive applications," in *Proceedings of the 11th International Symposium on Antenna Technology Applications [ANTEM 2005]*, pp. 1–4, Saint-Malo, France, June 2005.

[3] T. L. Chiu, L. Huitema, O. Pajona, and T. Monediere, "Compact and multiband MIMO dielectric resonator antenna for automotive LTE communications," *International Journal of Antennas and Propagation*, vol. 2018, Article ID 8231081, 15 pages, 2018.

[4] A. Ahmad, D. y. Choi, and S. Ullah, "A compact two elements MIMO antenna for 5G communication," *Scientific Reports*, vol. 12, p. 3608, 2022.

[5] A. Khan, S. Geng, X. Zhao, Z. Shah, M. U. Jan, and M. A. Abdelbaky, "Design of mimo antenna with an enhanced isolation technique," *Electronics*, vol. 9, no. 8, pp. 1217–17, 2020.

[6] L. Zhao, L. Liu, Y. M. Cai, and Y. M. Cai, "A MIMO antenna decoupling network composed of inverters and coupled split ring resonators," *Progress in Electromagnetics Research C*, vol. 79, pp. 175–183, 2017.

[7] N. Yamaki and N. Honma, "Simple design of decoupling network considering mutual admittance in array antenna," in *Proceedings of the 2011 International Symposium on Antennas Propagation (ISAP 2011), Electric Proc. of ISAP 2011*, Morioka, Japan, August 2011.

[8] H. Alwareth, I. M. Ibrahim, Z. Zakaria, A. J. A. Al-Gburi, S. Ahmed, and Z. A. Nasser, "A wideband high-gain microstrip array antenna integrated with frequency-selective

surface for Sub-6 GHz 5G applications," *Micromachines*, vol. 13, no. 8, p. 1215, 2022.

[9] R. H. Alhawari, T. Saeidi, A. H. M. Almawgani et al., "Wearable metamaterial dual-polarized high isolation UWB MIMO vivaldi antenna for 5G and satellite communications," *Micromachines*, vol. 12, p. 1559, 2021.

[10] M. Khalid, S. Iffat Naqvi, N. Hussain et al., "4-Port MIMO antenna with defected ground structure for 5G millimeter wave applications," *Electronics*, vol. 9, no. 1, p. 71, 2020.

[11] J. T. Ali, J. Iqbal, U. Illahi et al., "Mutual coupling reduction through defected ground structure in circularly polarized, dielectric resonator-based MIMO antennas for sub-6 GHz 5G applications," *Micromachines*, vol. 13, p. 1082, 2022.

[12] P. Kumar and T. Ali, "Characteristic mode analysis-based compact dual band-notched UWB MIMO antenna loaded with neutralization line," *Micromachines*, vol. 13, p. 1599, 2020.

[13] R. Liu, X. An, H. Zheng, M. Wang, Z. Gao, and E. Li, "Neutralization line decoupling tri-band multiple-input multiple-output antenna design," *IEEE Access*, vol. 8, Article ID 27018, 2020.

[14] B. Punna and P. Muthusamy, "Printed MIMO/diversity antenna with polarization diversity," *Progress in Electromagnetics Research Letters*, vol. 99, pp. 25–33, 2021.

[15] B. Zhang, J. Ren, Y. X. Sun, Y. Liu, and Y. Yin, "Four-port cylindrical pattern-and polarization-diversity dielectric resonator antenna for MIMO application," *IEEE Transactions on Antennas and Propagation*, vol. 70, no. 8, pp. 7136–7141, 2022.

[16] O. Y. Kwon, R. Song, and B. S. Kim, "A fully integrated shark-fin antenna for MIMO-LTE, GPS, WLAN, and WAVE applications," *IEEE Antennas and Wireless Propagation Letters*, vol. 17, no. 4, pp. 600–603, 2018.

[17] M. Gallo, S. Bruni, and D. Zamberlan, "A novel fully integrated fin antenna for automotive application," in *Proceedings of the 8th European Conference Antennas Propaganation. EuCAP*, pp. 2986–2989, Netherlands, Europe, April 2014.

[18] Y. Liu, Z. Ai, G. Liu, and Y. Jia, "An integrated shark-fin antenna for MIMO-LTE, FM, and GPS applications," *IEEE Antennas and Wireless Propagation Letters*, vol. 18, no. 8, pp. 1666–1670, 2019.

[19] T. Zhu, G. Ji, G. Jiang, Y. Ding, J. Feng, and C. Wang, "Comparing and analysis of test and evaluation methods for connected vehicle communication antenna system," *Journal of Physics: Conference Series*, vol. 2108, no. 1, Article ID 012007, 2021.

[20] L. Kannappan, S. K. Palaniswamy, M. Kanagasabai et al., "3-D twelve-port multi-service diversity antenna for automotive communications," *Scientific Reports*, vol. 12, no. 1, p. 403, 2022.

[21] L. Kannappan, S. K. Palaniswamy, M. Kanagasabai, S. Kumar, T. R. Rao, and T. Govindan, "Sub-6 GHz eight-port 3-D vehicular antenna," in *Proceedings of the 2022 International Conference on Wireless Communications Signal Processing and Networking (WiSPNET)*, pp. 293–296, Chennai, India, March 2022.

[22] A. Desai, C. D. Bui, J. Patel, T. Upadhyaya, G. Byun, and T. K. Nguyen, "Compact wideband four element optically transparent MIMO antenna for mm-wave 5G applications," *IEEE Access*, vol. 8, Article ID 194206, 2020.

[23] A. Desai, M. Palandoken, J. Kulkarni, G. Byun, and T. K. Nguyen, "Wideband flexible/transparent connected-ground MIMO antennas for sub-6 GHz 5G and WLAN applications," *IEEE Access*, vol. 9, Article ID 147003, 2021.

[24] A. Desai, T. Upadhyaya, M. Palandoken, and C. Gocen, "Dual band transparent antenna for wireless MIMO system applications," *Microwave and Optical Technology Letters*, vol. 61, no. 7, pp. 1845–1856, 2019.

[25] N. Jaglan, S. D. Gupta, E. Thakur, D. Kumar, B. K. Kanaujia, and S. Srivastava, "Triple band notched mushroom and uniplanar EBG structures based UWB MIMO/Diversity antenna with enhanced wide band isolation," *AEU-International Journal of Electronics and Communications*, vol. 90, pp. 36–44, 2018.

[26] N. Jaglan, B. K. Kanaujia, S. D. Gupta, S. Srivastava, and S. Srivastava, "Dual band notched EBG structure based UWB MIMO/diversity antenna with reduced wide band electromagnetic coupling," *Frequenz*, vol. 71, no. 11, pp. 555–565, 2017.

[27] N. Jaglan, B. K. Kanaujia, S. D. Gupta, and S. Srivastava, "Design of band-notched antenna with DG-CEBG," *International Journal of Electronics*, vol. 105, no. 1, pp. 58–72, 2018.

[28] M. S. Sharawi, "Current misuses and future prospects for printed multiple-input, multiple-output antenna systems [wireless corner]," *IEEE Antennas and Propagation Magazine*, vol. 59, no. 2, pp. 162–170, April 2017.

[29] T. Govindan, S. K. Palaniswamy, M. Kanagasabai, S. Kumar, T. Rama Rao, and M. G. N. Alsath, "Conformal quad-port UWB MIMO antenna for body-worn applications," *International Journal of Antennas and Propagation*, vol. 2021, Article ID 9409785, 13 pages, 2021.

[30] L. C. Tsai, "A dual-band bow-tie-shaped CPW-fed slot antenna for WLAN applications," *Progress in Electromagnetics Research C*, vol. 47, pp. 167–171, 2014.

[31] R. Krishnamoorthy, A. Desai, R. Patel, and A. Grover, "4 Element compact triple band MIMO antenna for sub-6 GHz 5G wireless applications," *Wireless Networks*, vol. 27, no. 6, pp. 3747–3759, 2021.

[32] G. Saxena, Y. K. Awasthi, and P. Jain, "Four-element pentaband MIMO antenna for multiple wireless application including dual-band circular polarization characteristics," *International Journal of Microwave and Wireless Technologies*, vol. 14, no. 4, pp. 465–476, 2022.

[33] N. K. Kiem, H. N. B. Phuong, and D. N. Chien, "Design of compact 4×4 UWB-MIMO antenna with WLAN band rejection," *International Journal of Antennas and Propagation*, vol. 2014, pp. 1–11, Article ID 539094, 2014.

[34] L. Kannappan, S. K. Palaniswamy, L. Wang et al., "Quad-port multiservice diversity antenna for automotive applications," *Sensors*, vol. 21, no. 24, p. 8238, 2021.

[35] U. D. Yalavarthi, "Reconfigurable orthogonal quad-port MIMO antenna for DSRC, WLAN, RADAR and Ku-band applications," *AEU International Journal of Electronics and Communications*, vol. 136, Article ID 153766, 2021.

[36] R. Mathur and S. Dwari, "Frequency and port reconfigurable MIMO antenna for UWB/5G/WLAN band IoT applications," *International Journal of RF and Microwave Computer-Aided Engineering*, vol. 31, no. 7, 2021.